# Application of up-sampling and resolution scaling to Fresnel reconstruction of digital holograms

Logan A. Williams,[1] Georges Nehmetallah,[2] Rola Aylo,[3] and Partha P. Banerjee[1,*]

[1]Electro-Optics Program, University of Dayton, Dayton, Ohio 45469, USA

[2]Electrical Engineering and Computer Science, Catholic University of America, Washington DC 20064, USA

[3]Electrona Engineering LLC, 430 Taylor St. N.E., Washington DC 20017, USA

*Corresponding author: pbanerjee1@udayton.edu

Received 17 September 2014; revised 8 January 2015; accepted 12 January 2015;
posted 16 January 2015 (Doc. ID 223395); published 18 February 2015

Fresnel transform implementation methods using numerical preprocessing techniques are investigated in this paper. First, it is shown that up-sampling dramatically reduces the minimum reconstruction distance requirements and allows maximal signal recovery by eliminating aliasing artifacts which typically occur at distances much less than the Rayleigh range of the object. Second, zero-padding is employed to arbitrarily scale numerical resolution for the purpose of resolution matching multiple holograms, where each hologram is recorded using dissimilar geometric or illumination parameters. Such preprocessing yields numerical resolution scaling at any distance. Both techniques are extensively illustrated using experimental results. 

*OCIS codes:* (090.1995) Digital holography; (100.3010) Image reconstruction techniques.
http://dx.doi.org/10.1364/AO.54.001443

## 1. Introduction

In digital holography (DH), holograms are formed through the interference of the diffracted light from an object and a reference beam on an imaging device such as a CCD [1–7]. This interference pattern is sampled by the CCD, and the Huygens–Fresnel diffraction integral using the Fresnel transform method (FTM), convolution integral method (CIM), or angular spectrum method (ASM) are often used for numerical reconstruction of this sampled hologram [1–11]. These techniques share a common feature where the spatial resolution of the reconstructed image is limited by the number and size of the pixels of the CCD [11]. However, the FTM is one of the most common and computationally efficient forms of image reconstruction in DH, and is used for longer reconstruction distances, in contrast to CIM or ASM which can be used for relatively shorter reconstruction distances [12]. The Fresnel transform asserts certain limitations upon the recording geometry, including an inability to adequately reconstruct fields recorded below a certain minimum object-to-CCD distance to maintain the paraxial approximation inherent in the FTM [1,2,9,11]. Additionally, the reconstructed image resolution is predetermined by the physical recording parameters, which may not necessarily provide the desired resolution for a given application.

Extensive research has been conducted to improve resolution of the reconstructed digital hologram through innovative techniques. One of these techniques is phase shifting digital holography, which can reconstruct an arbitrary view of a 3D object with improved image quality or a wider field of view compared to conventional DH using an off-axis configuration [13,14]. Another technique is to use an off-axis DH setup with a synthetic aperture [15]. The aperture is constructed from camera recordings at different positions and an algorithm to reconstruct each section shows an improved overall resolution.

1559-128X/15/061443-10$15.00/0

A third approach to enhance resolution employs placing a diffraction grating in front of the object. The grating ensures that more diffracted object waves reach the CCD, thus enhancing the diffraction-limited resolution [16]. A fourth method uses direct course sampling of holograms for wavefront reconstruction, where the number of required samples is reduced by the ratio of the carrier frequency signal to twice the signal bandwidth [17].

In this paper, we examine simple numerical preprocessing techniques that can be used to improve the performance of FTM during numerical reconstruction of a digital hologram. The first is to eliminate the restriction of long reconstruction distance from the Fresnel transform by use of up-sampling through interpolation of the recorded digital hologram. The "advantage" to this method is that it adds yet another way to reconstruct at small distances (near-field), beyond the angular spectrum or compressive sensing methods. The proposed method is a "numerical" improvement of resolution at short distances. It does not increase "absolute" resolution (i.e., it cannot resolve beyond the diffraction limit). In Section 2, the traditional limits of the FTM are discussed. In Section 3, the use of up-sampling through interpolation is then proposed as a means to reduce the reconstruction (and hence, recording) distance, followed by various illustrative examples in Section 4. As a second preprocessing technique to improve FTM, the benefits of arbitrary resolution scaling are discussed in Section 5, which can be useful not only in multiwavelength digital holography (MWDH), but also, for instance, in single-shot multiple projection holographic tomography with different recording distances. Section 6 concludes this paper.

## 2. Traditional Limits of the Fresnel Transform

It is well known that the usefulness of the Fresnel transform in DH reconstruction is generally limited to distances beyond the near-field, where the recording (and hence, reconstruction) distance $d$ is approximately equal to, or greater than, $d_{\min} \approx z_R = \pi l^2/\lambda$, where $l$ is the "feature size" of the object, and $\lambda$ is the illumination wavelength. Called the Rayleigh range for a Gaussian beam, $z_R$ is simply the distance at which the Fresnel number $F = \frac{l^2}{\lambda d} = 1/\pi$. This minimum recording distance, $d_{\min}$, is the typical near-object reconstruction limit of the Fresnel transform, as shown in Fig. 1.

On the other hand, in the hologram recording process, a geometrical argument to determine the minimum value of $d$ based upon the maximum angular frequency recorded using an in-line geometry is also given by Schnars and Jueptner [1], which is

$$d_{\min} \approx \frac{r_{\max}}{\theta_{\max}} = \sqrt{2}\frac{\Delta x}{\lambda}(L_{\text{obj}} + N\Delta x), \qquad (1)$$

where $\Delta x$ is the pixel pitch of the CCD and $N$ is the number of pixels along the $\Delta x$ direction, $r_{\max}$ is the maximum path length from the farthest transverse extent of the object of size $L_{\text{obj}}$ to the farthest transverse extent of the CCD array, and $\theta_{\max}$ is the maximum diffraction angle captured by the CCD array, as shown in Fig. 2. Equation (1) is derived based upon an in-line geometry, though the specific form of $r_{\max}/\theta_{\max}$ will vary with different geometries (e.g., off-axis recording), such that $d_{\min}$ typically increases as the object moves further off-axis. Note that for all other setups the maximum spatial frequency that can be recorded by the CCD to avoid aliasing by the CCD has to be adapted very carefully to the resolution of that particular CCD. If too high spatial frequencies occur, the contrast of the entire hologram decreases.

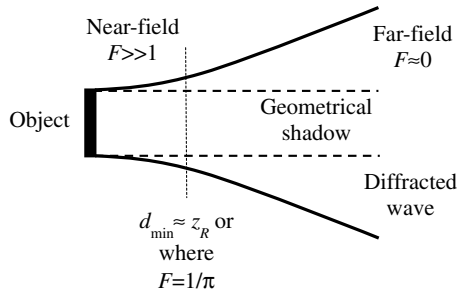


Fig. 1. Illustration of near- and far-field diffraction zones, along with minimum reconstruction distance $d_{\min} \approx z_R$, the Rayleigh range. The dashed lines show the geometrical shadow of the object, solid lines represent spreading due to diffraction.

However, both of these criteria are only heuristic. The actual limitation on $d$ is determined more rigorously by the extent of the spatial bandwidth of the object field that can be effectively captured by the CCD array under the Whittaker–Shannon sampling theorem [8]. If $d < d_{\min}$, alternative reconstruction methods may be employed (e.g., ASM) to faithfully reconstruct the image. This fact reveals that the image information has indeed been recorded by the CCD at these distances; it is simply not recoverable via standard implementation of the Fresnel transform, as given in [1]. Differences between Fresnel reconstruction and the angular spectrum method (or Rayleigh–Sommerfeld diffraction formulation) for sampled diffraction fields have been analyzed by Onural who concluded that both techniques have the expected higher diffraction orders translated to the same locations, modulated by the same complex sinusoidals, but there is no dispersion in the FTM case [18].

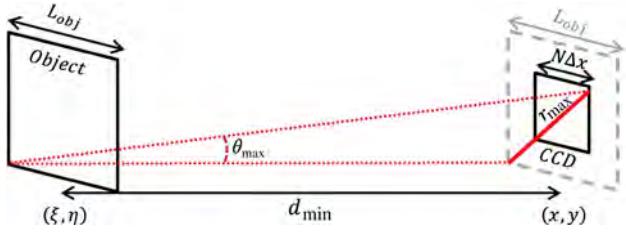


Fig. 2. Pseudo-3D illustration of the recording geometry given by Eq. (1). In this case, the maximum path length is the transverse projection, $r_{\max}$, on the CCD plane of the path from the lower left corner of the object to the upper right corner of the CCD array [1].

### 3. Reduction of the Reconstruction Distance

It is possible to illustrate the effect of numerical up-sampling on the reconstruction distance by examining the total signal bandwidth sampled by the CCD. For Fresnel holograms, Goodman [8] has shown that the captured bandwidth of the hologram field, $B_x$, is related to two factors: (a) the size of the object which determines the bandwidth of the hologram field, and therefore in turn determines the number of hologram field samples required (the first component of the bandwidth), and (b) the bandwidth of the quadratic-phase factor in $(x,y)$, or the kernel (the second component of the bandwidth). Since these two factors are multiplied in space, the corresponding bandwidths are added in the spatial frequency domain due to convolution. Adding these two effects together results in

$$B_x = \frac{L_\xi}{2\lambda d} + \frac{L_x}{2\lambda d}, \tag{2}$$

where $L_\xi$ and $L_x$ are the total array lengths in the $\xi$ (image plane) and $x$ (hologram plane) directions, such that $L_\xi = N_\xi \cdot \Delta\xi$ and $L_x = N_x \cdot \Delta x$, where $N_\xi$ and $N_x$ are the number of samples in the $\xi$ and $x$ directions, respectively. Properties of the discrete Fourier transform (DFT) dictate that $N_\xi = N_x \equiv N$. The minimum sampling interval (pixel size) for a given bandwidth dictated by the Whittaker–Shannon sampling theorem is

$$\Delta x = \frac{1}{2B_x}, \tag{3}$$

such that the total number of required samples is given by [8]

$$N = \frac{L_x}{\Delta x} = \frac{L_x(L_x + L_\xi)}{\lambda d} = \frac{L_x^2}{\lambda d} + \frac{L_x L_\xi}{\lambda d}. \tag{4}$$

Therefore, the CCD array size and fixed pixel pitch generally determine the maximum recoverable bandwidth. While this analysis concerns only the $\xi$ and $x$ directions, an equivalent analysis may be performed on the orthogonal $\eta$ and $y$ directions in the respective image and hologram planes.

From Eq. (4) it may be noticed that if the value of $N$ is increased while $L_\xi$ and $L_x$ are held constant, the value of $d$ may be correspondingly reduced by the same degree while still satisfying the sampling theorem. Such is the case if the recorded hologram matrix is numerically up-sampled via bicubic interpolation [19]. In this case, $N$ is increased by a scaling factor $\zeta$, while $\Delta x$ is reduced by the same factor, such that $L_\xi$ and $L_x$ remain constant:

$$L_\xi = \zeta \cdot N \cdot \left(\frac{\Delta\xi}{\zeta}\right), \qquad L_x = \zeta \cdot N \cdot \left(\frac{\Delta x}{\zeta}\right). \tag{5}$$

The numerical effect of increasing $N$ while maintaining the same total physical extent is that it increases the sampling rate, which is equivalent to reducing the pixel pitch, thus allowing the Fresnel transform to be accurately calculated at the reduced distance. The numerical resolution of the new reconstruction (based upon the up-sampled hologram) is still determined by the reconstruction distance, $d$, the physical array size, and illumination wavelength, given by the familiar equation

$$\Delta\xi = \frac{\lambda d}{L_x}, \tag{6}$$

in which $L_x$ remains constant. Note that Eq. (6) is based upon the diffraction-limited resolution of the holographic recording configuration, which dictates the resolution limit (Airy disk radius) in the reconstructed object plane [1]. Thus, numerical up-sampling does not increase the "absolute" resolution of the reconstruction, but allows the image to be reconstructed at small distances that have been traditionally forbidden due to excessive image aliasing.

A more rigorous mathematical treatment of this principle is given by Kelly *et al.* [20], where it is shown that the CCD pixel spacing $\Delta x$ directly determines, via an inverse Fourier relationship, the spacing between reconstructed image replicas, and thus the degree of overlap, or aliasing, of the reconstructed image. However, in this method rather than altering the sampling rate (i.e., pixel spacing, $\Delta x$) physically at the CCD, it is altered numerically prior to Fresnel reconstruction. This allows the maximal recorded spatial bandwidth to be reconstructed, unaliased, directly via Fresnel transform rather than some other method (i.e., CIM, ASM, and compressive sensing). However, numerical up-sampling does not improve or otherwise alter the physical limitations imposed by the finite extent of each CCD pixel, as discussed in [20], and is not able to recover the evanescent field of the object, regardless of the reduction in recording/reconstruction distance.

A mathematical proof of this up-sampling effect is given below using Fourier analysis. Assuming one transverse coordinate for simplicity, the recording process involves the convolution of the complex field from the original object $o(\xi)$ with the free-space spatial impulse response of propagation. The expression for the recorded intensity on the CCD plane, which is the interference of this Fresnel propagated complex field with a reference wave (assumed to be uniform amplitude and taken to be 1 for simplicity), and therefore proportional to $|1 + o_F(x)|^2$, contains the term

$$o_F(x) = \left[o(\xi) * e^{-\frac{jk_0\xi^2}{2d}}\right]\Bigg|_{\xi=x} \propto \mathrm{FT}^{-1}\left[O(k_x)e^{\frac{jk_x^2 d}{2k_0}}\right], \tag{7}$$

where $k_0$ is the propagation constant, and $o_F(x)$ is the Fresnel propagated object field at the CCD. In Eq. (7), $\mathrm{FT}^{-1}$ denotes the inverse (spatial) Fourier transform [with $O(k_x)$ denoting the forward Fourier transform of $o(x)$] [8,21–24], the recording (and reconstruction) distance is $d$, and $k_x$ denotes a spatial

frequency variable. Also, in writing the last term in Eq. (7), we have left out a constant multiplier for the sake of simplicity. The forward Fourier transform is defined as $\mathrm{FT}\{f(x)\} = F(k_x) = \int_{-\infty}^{\infty} f(x)e^{jk_x x}dx$, with the inverse transform being $\mathrm{FT}^{-1}\{F(k_x)\} = f(x) = \frac{1}{2\pi}\int_{-\infty}^{\infty} F(k_x)e^{-jk_x x}dk_x$.

The pixelated CCD records this information as

$$o_{Fp}(x) \propto \left[\left[o_F(x)\mathrm{comb}\left(\frac{x}{\Delta x}\right)\right] * \mathrm{rect}\left(\frac{x}{\Delta x}\right)\right]\mathrm{rect}\left(\frac{x}{L_x}\right), \tag{8}$$

where the comb function along with the convolving rect function describe the sampling at the CCD plane with pixel pitch $\Delta x$. The last rect function describes the size $L_x = N\Delta x$ of the CCD. Equation (8) indicates that the CCD samples the values of the Fresnel propagated field at the locations of the delta functions comprising the comb function and retains this value over the size of the pixel.

The component of the Fresnel reconstruction of the digital hologram recorded on the CCD at a reconstruction distance $-d$ resulting from the information recorded in Eq. (8) should yield the virtual image of the object. This operation, which is usually performed through back-propagation using the Fresnel diffraction formula, can be mathematically expressed as

$$o'(\xi) \propto e^{jk_0\xi^2/2d}\mathrm{FT}\left\{o_{Fp}(x)e^{jk_0x^2/2d}\right\}\Big|_{k_x=-k_0\xi/d}, \tag{9}$$

where $o'(\xi)$ is the reconstructed virtual image [mathematically different from $o(\xi)$]. The last exponential denotes a multiplier to the recorded optical field, which, along with the scaled FT operation, simulates the commonly used back-propagation algorithm for the reconstruction distance $-d$ using the Fresnel diffraction formula [8,11,24]. The scaling is given by $k_x = -k_0\xi/d$, where $\xi$ is the image plane coordinate.

Combining all the previous steps from Eqs. (7) to (9) we arrive at a single equation for the reconstructed virtual image of the following form:

$$o'(\xi) \propto e^{jk_0\xi^2/2d}\mathrm{FT}\left\{\left[\left(\mathrm{FT}^{-1}\left[O(k_x)e^{\frac{jk_x^2 d}{2k_0}}\right]\mathrm{comb}\left(\frac{x}{\Delta x}\right)\right) * \mathrm{rect}\left(\frac{x}{\Delta x}\right)\right]\mathrm{rect}\left(\frac{x}{L_x}\right)e^{jk_0x^2/2d}\right\}\Big|_{k_x=-k_0\xi/d} \tag{10}$$

The objective is to show that by up-sampling or increasing $N$, or, equivalently, decreasing $\Delta x$ (while keeping $L_x$ constant), faithful reconstruction can be performed for smaller reconstruction distances $d$.

It can be readily shown after some algebra that as $\Delta x \to 0$, the FT operation in Eq. (10), before the substitution $k_x = -k_0\xi/d$, can be approximated as being proportional to

$$\left(O(k_x)e^{\frac{jk_x^2 d}{2k_0}}\right) * e^{\frac{jk_x^2 d}{2k_0}} * \mathrm{comb}\left(\frac{k_x}{2\pi/\Delta x}\right). \tag{11}$$

In deriving Eq. (11), it has been assumed that $\mathrm{FT}[\mathrm{rect}(\frac{x}{\Delta x})]$ is approximately a constant, and that $\mathrm{rect}(\frac{x}{L_x}) \approx 1$ over the "effective" extent of the comb function $\mathrm{comb}(\frac{x}{\Delta x})$. Also, use has been made of the associative property of convolution $a * (b * c) = a * b * c = (a * b) * c$. The first convolution in Eq. (11) can be expressed as being proportional to $o(-\frac{k_x d}{k_0})e^{-j\frac{k_x^2 d}{2k_0}}$, so that Eq. (11) can be re-expressed as being proportional to

$$e^{jk_0\xi^2/2d}\left[\left[o\left(-\frac{k_x d}{k_0}\right)e^{-j\frac{k_x^2 d}{2k_0}}\right] * \mathrm{comb}\left(\frac{k_x}{2\pi/\Delta x}\right)\right]\Big|_{k_x=-k_0\xi/d}. \tag{12}$$

It is to be noted that without the comb function, Eq. (12) yields $o(\xi)$, which is the reconstructed object with appropriate coordinates. Therefore, the result in Eq. (12) can be interpreted as the convolution of the object with a comb function. As $\Delta x$ becomes smaller, the separation between successive delta functions comprising the *comb* function increases. Smaller reconstruction distances $d$, which (inversely) scale the size of the object, are therefore now possible, since the scaled object can be accommodated around successive delta functions without aliasing. A larger $\Delta x$ would require larger values for $d$, thus supporting the hypothesis that up-sampling does, indeed, facilitate shorter recording and reconstruction distances using the Fresnel diffraction formula. Unambiguous reconstruction is achieved on the image plane when the separation between the delta functions in Eq. (12) equals the array length $L_\xi = N\Delta\xi$. This condition simplifies to $\Delta\xi = \frac{\lambda d}{N\Delta x} = \frac{\lambda d}{L_x}$, which is identical to Eq. (6), and determines the numerical resolution of the reconstruction independent of the up-sampling, as mentioned above.

It should be understood that the highest spatial frequency information to be reconstructed must necessarily be recorded by the CCD to produce an adequate reconstruction. The bicubic up-sampling cannot "add" high frequency information which was not recorded by the CCD array. The up-sampling procedure can only add pixels via interpolation,

thus increasing the "resolution" of the information already present by altering the spacing between the reconstruction centers in the up-scaled reconstruction. However, interpolation cannot add new content or recover higher frequency content than that initially recorded by the CCD. This numeric reduction in pixel pitch reduces aliasing by increasing the distance between reconstruction centers, but does not alter the originally recorded spatial bandwidth.

## 4. Illustrative Experimental Results

The reduction of reconstruction distance through up-sampling has been verified by recording and reconstruction of holograms of several objects. Here, two illustrative examples are discussed.

**Example 1**:

The first example shown here is that of a tungsten filament of coil diameter 300 μm ($z_R \approx 11$ cm for $\lambda = 632.8$ nm) for which inline holograms have been recorded at various distances, and Fresnel transform reconstructions performed both with and without bicubic up-sampling of $N_x$ and $N_y$ using the geometry shown in Figs. 3(a) and 3(b). A Lumenera CCD camera (LU-120M) consisting of a $1024 \times 1024$ pixel array is used, with a physical pixel size of $\Delta x = 6.7$ μm. The original hologram size is cropped to $200 \times 200$ pixels before up-sampling by a factor of $\zeta = 6$ to $1200 \times 1200$ pixels, with an equivalent pixel size of $\Delta x/\zeta = 1.12$ μm. The reconstructed image is therefore also $1200 \times 1200$ pixels, with numerical resolution of $\Delta\xi = 1.17$ μm. Because $\Delta\xi$ depends only on recording and reconstruction distance, the value of $\Delta\xi$ remains the same with or without numerical up-sampling, although the effect of aliasing changes dramatically. Figures 4(a)–4(d) compare Fresnel transform reconstructions of unscaled and up-sampled ($\zeta = 6$) holograms recorded at $d = 2.5$ mm. Note that for weakly scattering in-line holograms recorded at $d \ll z_R$, cropping the recorded hologram serves only to limit the lateral extent of both the recorded and reconstructed holograms. This is due to the fact that under the $d \ll z_R$ condition diffracted waves from nonadjacent regions of the object exceed $\theta_{\max}$, resulting in exceptionally weak interference that surpasses the bandwidth recording capabilities of the CCD, as given by Eq. (1) and illustrated in Fig. 2. Additionally, cropping is necessary to limit the overall up-sampled hologram size to avoid computational memory limitations.

The reduction in reconstruction distance to $d = 2.5$ mm is rather dramatic considering the fact that $z_R \approx 11$ cm (assuming feature size equal to the coil radius), or the geometrical argument of Eq. (1) that yields $d_{\min} \approx 10.5$ cm. Indeed, the Fresnel transform (using native resolution) begins to adequately reconstruct this object when recorded at a distance greater than about $d = 10$ cm, albeit rather poorly, with a corresponding resolution of $\Delta\xi = 47$ μm (see Section 5). It has been experimentally verified that with a scaling factor of $\zeta = 15$, the recording/reconstruction distance can be reduced to $d \approx 500$ μm, which places this object directly on the CCD cover glass (not shown). It should be noted that, although numerical values for $\Delta\xi$ can be made arbitrarily small using numerical methods, in all cases the limiting physical resolution of the reconstructed image is dictated by diffraction of the object wave, which in turn is limited by the angular spectrum physically recorded by the CCD.

**Example 2**:

The second example shown is that of a dandelion, whose hologram is shown in Fig. 5(a), along with the reconstructions without and with bicubic up-sampling by a factor $\zeta = 7$, as shown in Figs. 5(b) and 5(c), respectively. In this case, the thickness of the dandelion wing is approximately 30 μm ($d_{\min} \approx 12$ cm for $\lambda = 543.5$ nm), and the recording distance is approximately 6.6 mm. For comparison, reconstruction using the (nonparaxial) transfer function method, as reported in Banerjee *et al.* [25], is shown in Fig. 5(d). As is apparent from the reconstructions, the use of up-sampling removes aliasing and yields results comparable to, and perhaps better (with respect to elimination of twin images) than, the nonparaxial transfer function method; this is currently under study.

It is also to be noted that the bicubic up-sampling technique is primarily applicable to a lensless, or Fresnel hologram, as given by the geometry of Fig. 3(a). In the case of a Fourier hologram, using a lens, the hologram recording is dependent upon a fixed distance, $f$, which is the lens focal length, rather than a variable distance, $d$. In this case, there is a direct Fourier transform relationship between the object and the hologram. The technique we describe here is used to eliminate aliasing artifacts caused by $d \ll z_R$. This technique is not applicable to Fourier recording configurations with fixed focal length, $f$, where the relationship between $d$ and $z_R$ is not applicable (since it is always equivalent to

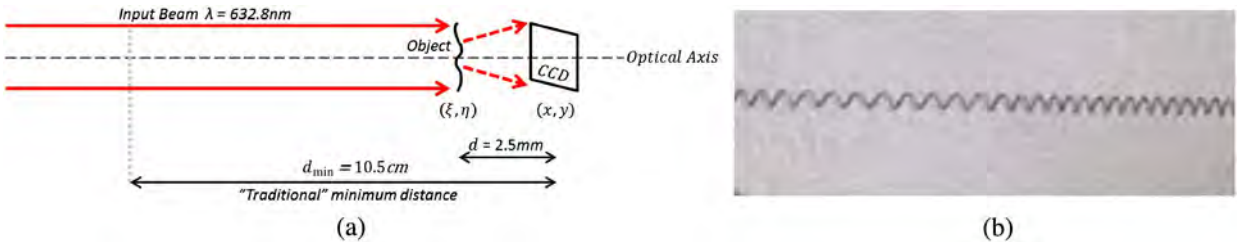


Fig. 3. (a) Near-field, in-line (Gabor) recording geometry, and (b) photograph of the tungsten filament object.

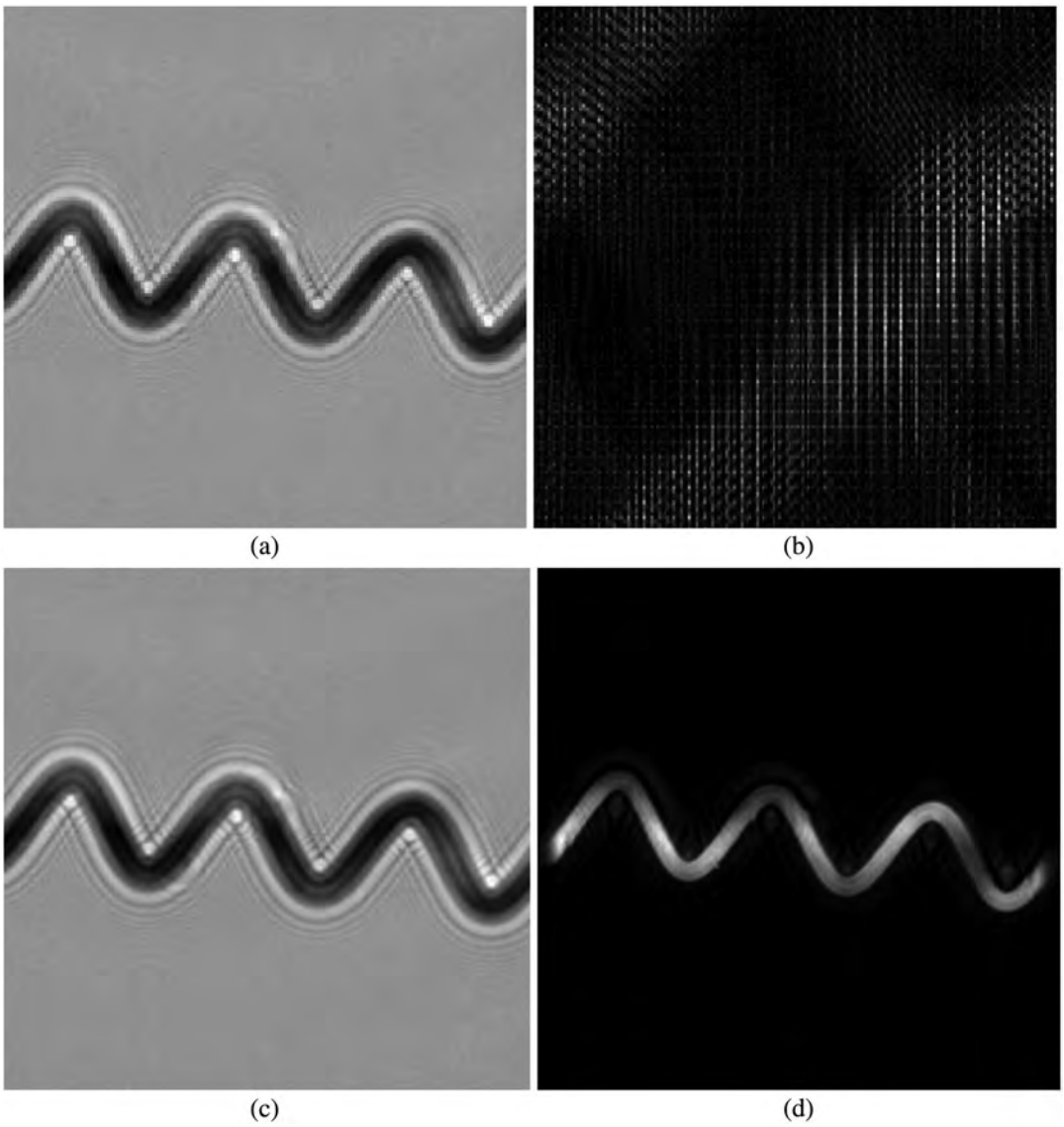


Fig. 4. (a) Recorded hologram (cropped to 200 × 200 pixels, $\Delta x = 6.7$ μm, image width = 1.34 mm) of a tungsten filament at $d = 2.5$ mm, (b) the highly aliased Fresnel reconstruction at $d = 2.5$ mm and $\Delta\xi = 1.17$ μm, using native CCD resolution $\Delta x = 6.7$ μm, (c) the up-sampled hologram (1200 × 1200 pixels), with scaling factor $\zeta = 6$ and pixel size $\Delta x/\zeta = 1.12$ μm, and (d) the unaliased Fresnel reconstruction at $d = 2.5$ mm using the up-sampled hologram, with numerical image resolution of $\Delta\xi = 1.17$ μm.

$d \gg z_R$ when placing the far-field at the focal plane of the lens). Basically, if the up-sampling technique is applied to a Fourier hologram, the image numerical resolution will scale with it (i.e., double the image size, pixel size is halved), but there will be no corresponding "improvement" of the image due to elimination of aliasing.

### 5. Arbitrary Resolution Scaling

It is also possible to scale the value of $N_x$ while keeping $\Delta x$ constant, such that $L_\xi$ and $L_x$ do not remain constant. This is accomplished by zero-padding the hologram prior to reconstruction. The resolution of the resulting reconstruction is still governed by Eq. (6), however, the size of $N_x$ (and subsequently, $L_x$) is now that of the zero-padded hologram. As $N_x$ increases, the value of $\Delta\xi$ decreases accordingly. In effect, zero-padding has artificially increased the numerical aperture of the system, allowing finer resolution of individual pixels, due to the inverse Fourier relationship between the full extent of the CCD array, $L_x$, and the size of each sample, $\Delta\xi$, in the reconstruction.

This method of resolution scaling allows the appearance of image reconstructions with relatively poor native resolution to be dramatically enhanced, as explored in Refs. [12,21,22,26–28], among others. This can be seen in Figs. 6(a)–6(d), in which the previous example is re-examined at $d = 10$ cm, near the limit of native Fresnel reconstruction, with $\Delta\xi = 47$ μm. However, after zero-padding the

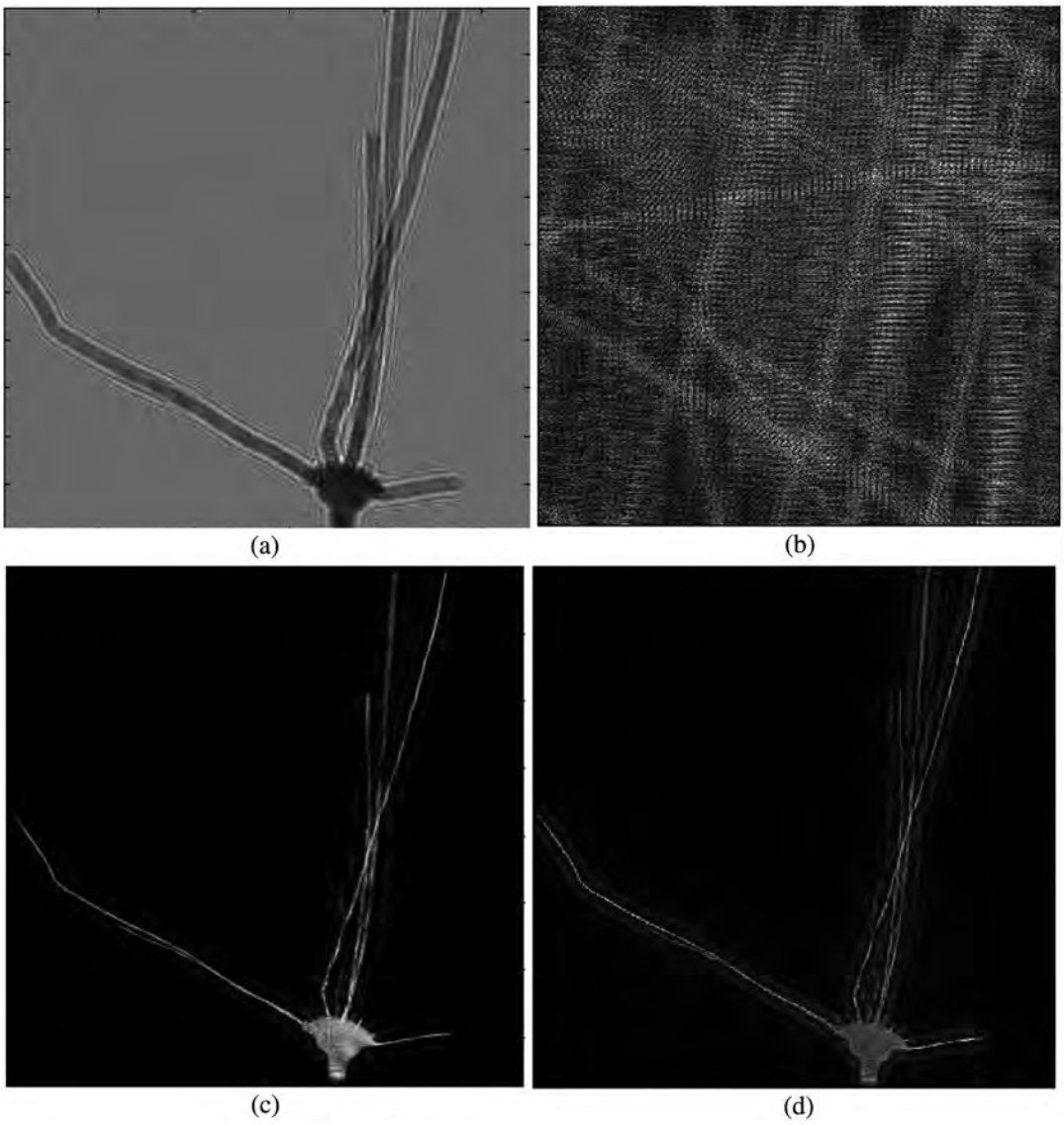


Fig. 5. (a) Recorded hologram (cropped to $551 \times 551$ pixels) of dandelion wings at $d = 6.6$ mm, (b) the highly aliased Fresnel reconstruction at $d = 6.6$ mm using native CCD resolution $\Delta x = 6.7$ μm, (c) the up-sampled hologram ($3857 \times 3857$ pixels), with scaling factor $\zeta = 7$ and pixel size $\Delta x/\zeta = 0.971$ μm, and (d) reconstruction using the nonparaxial transfer function method (ASM) at $d = 6.6$ mm with image resolution of $\Delta\xi = 6.7$ μm.

perimeter of the hologram by 600 indices, the image resolution is $\Delta\xi = 6.74$ μm. It should be noted that the recording was made at a distance $d \approx z_R$, which is at the limit of what could traditionally be called a "good" reconstruction.

Although this technique is generally well known, some applications of the usefulness of zero-padding to arbitrarily scale the reconstructed image resolution appear to be underrepresented in the literature. Notably, zero-padding allows the resolution of two holograms to be made equal when recorded using different parameters, $N_x$, $\lambda$, $d$, or $\Delta x$, which may be advantageous in a variety of applications. This is particularly useful when performing multiwavelength DH (MWDH), in which two holograms are recorded at separate wavelengths, $\lambda_1$ and $\lambda_2$. To effectively subtract the phases of two holograms, pixel-by-pixel, it must first be ensured that the pixel sizes of both holograms are equal, such that

$$\Delta\xi_1 = \frac{\lambda_1 d}{N_1 \Delta x} = \frac{\lambda_2 d}{N_2 \Delta x} = \Delta\xi_2, \tag{13}$$

where the subscripts 1 and 2 denote the hologram recordings made with either $\lambda_1$ or $\lambda_2$, respectively. If it is assumed that $\lambda_1 > \lambda_2$, then the $\lambda_1$ hologram (hologram #1) must be padded to reduce its resolution to equal that of hologram #2. The ratio of the initial resolutions is simply $\lambda_1/\lambda_2$, such that [26]

$$N_1 = \frac{\lambda_1}{\lambda_2} \cdot N_x, \tag{14}$$

where $N_x$ is the original size of either hologram array (i.e., without padding). Therefore, hologram #1 must

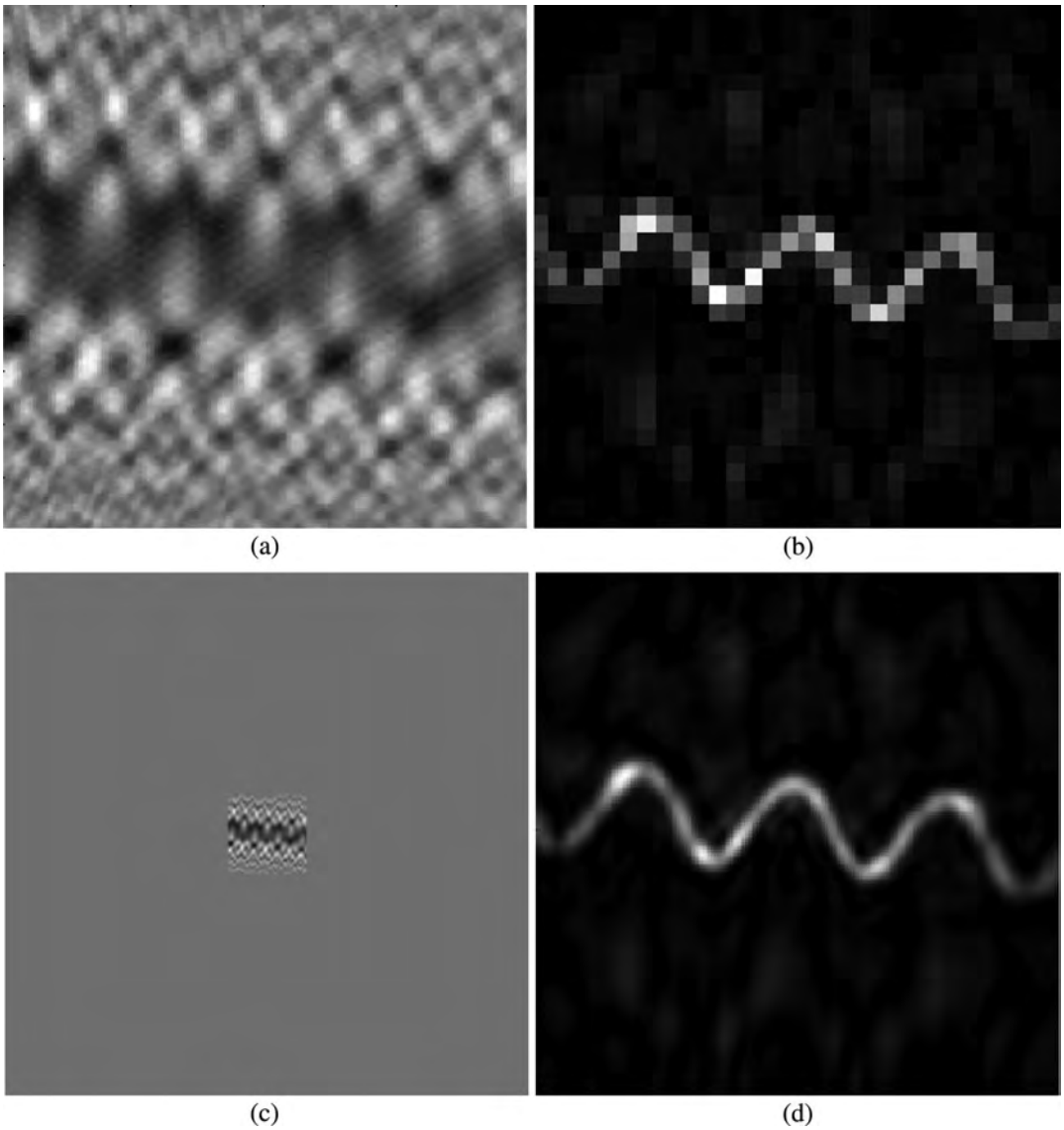


Fig. 6. (a) Recorded hologram (1024 × 1024 original size, cropped to 200 × 200 pixels, $\Delta x = 6.7$ μm, image width = 1.34 mm) of a tungsten filament at $d = 10$ cm, (b) the Fresnel reconstruction at $d = 10$ cm using native CCD resolution, with image resolution of $\Delta\xi = 47$ μm, (c) the zero-padded hologram, with 600 zero indices added to each border (1400 × 1400), and (d) the Fresnel reconstruction at $d = 10$ cm using the zero-padded hologram, with numerical resolution of $\Delta\xi = 6.74$ μm.

increase by a factor$(\frac{\lambda_1}{\lambda_2} - 1)$ with $\frac{1}{2}$ of the padding applied to each side of the $N_x \times N_y$ matrix. Thus, the amount of zero-padding which must be applied to each side of hologram #1 (for $N_x = N_y$) prior to reconstruction is given by

$$\text{pad size} = \text{round}\left[\frac{N_x}{2}\left(\frac{\lambda_1}{\lambda_2} - 1\right)\right], \tag{15}$$

where the rounding function ensures an integer number of indices. Reconstruction of the padded hologram #1 will result in equal resolution to that of hologram #2 (which is reconstructed without padding). However, the reconstructed size of hologram #1 is $N_1$, although the size of hologram #2 is still $N_x$. To simplify pixel-by-pixel subtraction, hologram #2 is padded post reconstruction to equal the size of $N_1$, which does not alter the value of $\Delta\xi_2$. This technique of padding has been used to determine the shape and volume of dents on a surface using MWDH, as shown in Williams *et al.* [29].

A similar procedure may be applied to resolution matching of holograms recorded with unequal values of $N_x$, $N_y$, $d$, $\Delta x$, or $\Delta y$. In addition to MWDH, such conditions arise in other applications, such as multiple projection holographic tomography, in which separate angular projections may be recorded at different distances as shown in the example below, or with different CCD arrays [30].

As shown in Ref. [30], single-shot multiple projection holographic tomography can be performed to

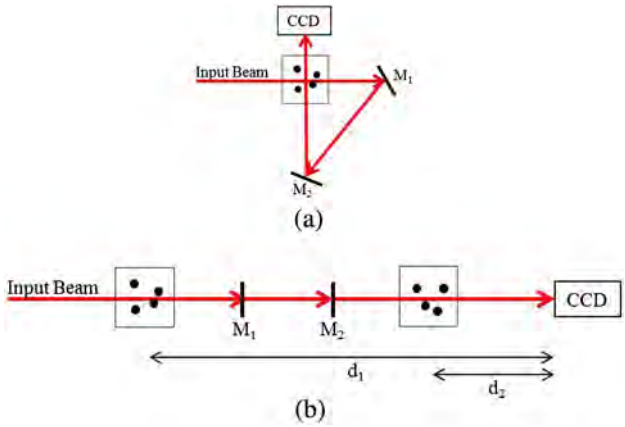


Fig. 7. (a) Schematic of single-shot multiple projection holographic tomography for recording and reconstructing the location of bubbles in water. (b) "Unfolded" version of the schematic in (a).

determine the 3D position of bubbles, using the schematic setup shown in Fig. 7(a). An "unfolded" version of the setup is shown in Fig. 7(b). The recording wavelength is $\lambda = 543.5$ nm, and $d_1 \approx 61.8$ cm, $d_2 \approx 20.6$ cm, and the CCD pitch is 6.7 μm. Owing to the double-pass of the light through two bubbles whose holograms are recorded, two sets of Fresnel holograms of these two bubbles are simultaneously registered on the CCD, with the larger sized holograms corresponding to the longer recording distance, as shown in Fig. 8(a). Bubble reconstruction using a cropped hologram with $422 \times 422$ pixels and reconstruction distance of $d_2 \approx 20.6$ cm yields Fig. 8(b) with a reconstructed pixel size of $\Delta\xi = 16.27$ μm. On the other hand, reconstruction of this hologram with a reconstruction distance of $d_1 \approx 61.8$ cm yields Fig. 8(c) with a reconstructed pixel size of $\Delta\xi = 48.82$ μm. However, by using

$$\text{pad size} = \text{round}\left[\frac{N_x}{2}\left(\frac{d_1}{d_2} - 1\right)\right], \tag{16}$$

the reconstructed pixel size can be restored to the desired value $\Delta\xi = 16.27$ μm, as shown in Fig. 8(d), which is essential in precisely determining the 3D location of the bubbles.

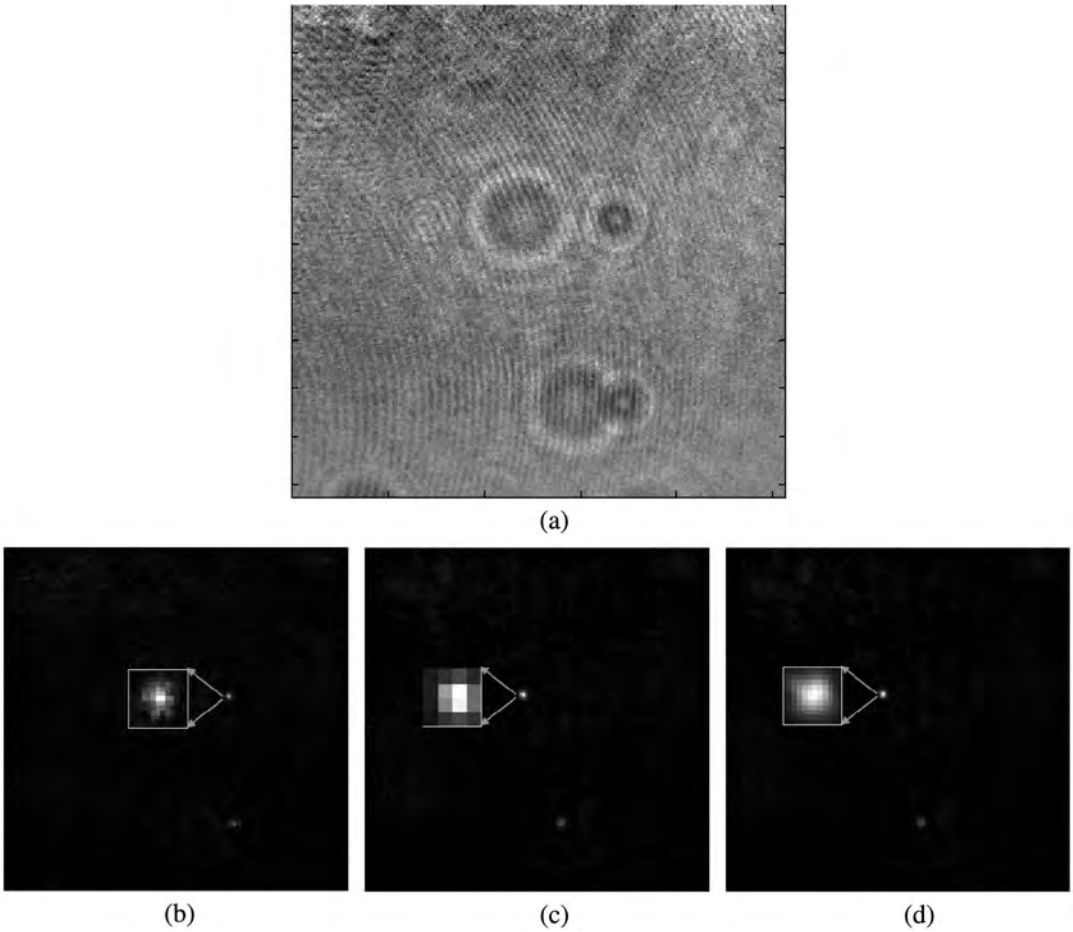


Fig. 8. (a) Recorded holograms ($1024 \times 1024$ pixels of pixel size 6.7 μm) of two bubbles using the single-shot multiple projection holographic tomography setup schematically shown in Fig. 7. Hologram reconstructions, cropped to show only the "on-axis" or "zero-order" field of view, for (b) reconstruction distance $d_2 \approx 20.6$ cm, ($422 \times 422$ pixels), (c) reconstruction distance $d_1 \approx 61.8$ cm, ($142 \times 142$ pixels), (d) reconstruction distance $d_1 \approx 61.8$ cm, and with zero-padding of 1024 pixels per side, cropped to $422 \times 422$ pixels. Insets in each of the figures (b)–(d) show respective reconstruction pixel size.

## 6. Conclusion

It has been experimentally shown that numerical preprocessing of the recorded hologram matrix, namely by up-sampling and zero-padding, can dramatically reduce the minimum reconstruction distance of the Fresnel transform while providing for arbitrary resolution scaling in the image plane. Using a simplified model, it has been shown that numerical up-sampling after hologram acquisition on a CCD camera can effectively reduce the reconstruction distance while preserving the numerical resolution of the reconstruction by overcoming the aliasing artifacts which typically occur at $d \ll z_R$. Also, it has been shown that judicious application of zero-padding (in the absence of aliasing) offers the capability to perform resolution matching and subsequent comparison of holograms recorded using different physical parameters, such as in MWDH and single-shot multi-angle holographic tomography. Zero-padding artificially increases the numerical aperture of the system, allowing finer resolution of individual pixels. The research presented here is an extension of preliminary results presented earlier [23]. While the bicubic up-sampling and zero-padding are two illustrative examples of numerical preprocessing, it is interesting to speculate on cases where both these methods of numerical preprocessing of Fresnel holograms can be combined. We plan to investigate this in the future.

We would like to thank the reviewers for their thorough reading of the manuscript and their very helpful comments.

## References

1. U. Schnars and W. Jueptner, *Digital Holography: Digital Hologram Recording, Numerical Reconstruction, and Related Techniques* (Springer, 2010).
2. U. Schnars and W. Juptner, "Digital recording and numerical reconstruction of holograms," Meas. Sci. Technol. **13**, R85 (2002).
3. T. Kreis, *Holographic Interferometry* (Academic, 1996).
4. T. Kreis, W. Juptner, and J. Geldmacher, "Digital holography: methods and applications," Proc. SPIE **3407**, 169–177 (1998).
5. T. Kreis, "Frequency analysis of digital holography," Opt. Eng. **41**, 771–778 (2002).
6. T. Kreis, "Frequency analysis of digital holography with reconstruction by convolution," Opt. Eng. **41**, 1829–1839 (2002).
7. M. K. Kim, "Principles and techniques of digital holographic microscopy," SPIE Rev. **1**, 018005 (2010).
8. J. Goodman, *Introduction to Fourier Optics*, 3rd ed. (Roberts & Company, 2005), p. 358.
9. U. Schnars and W. Juptner, "Direct recording of holograms by a CCD target and numerical reconstruction," Appl. Opt. **33**, 179–181 (1994).
10. L. P. Yaroslavskii and N. S. Merzlyakov, *Methods of Digital Holography* (Consultants Bureau, 1980).
11. G. Nehmetallah and P. P. Banerjee, "Applications of digital and analog holography in three-dimensional imaging," Adv. Opt. Photon. **4**, 472–553 (2012).
12. P. Ferraro, S. De Nicola, A. Finizio, G. Pierattini, and G. Coppola, "Recovering image resolution in reconstructing digital off-axis holograms by Fresnel transform method," Appl. Phys. Lett. **85**, 2709–2711 (2004).
13. I. Yamaguchi and T. Zhang, "Phase-shifting digital holography," Opt. Lett. **22**, 1268–1270 (1997).
14. T. Zhang and I. Yamaguchi, "Three-dimensional microscopy with phase-shifting digital holography," Opt. Lett. **23**, 1221–1223 (1998).
15. J. H. Massig, "Digital off-axis holography with a synthetic aperture," Opt. Lett. **27**, 2179–2181 (2002).
16. C. Liu, Z. Liu, F. Bo, Y. Wang, and J. Zhu, "Super-resolution digital holographic imaging method,"Appl. Phys. Lett. **81**, 3143–3145 (2002).
17. K. Khare and N. George, "Direct coarse sampling of electronic holograms," Opt. Lett. **28**, 1004–1006 (2003).
18. L. Onural, "Exact analysis of the effects of sampling of the scalar diffraction field," J. Opt. Soc. Am. A **24**, 359–367 (2007).
19. W. Press, S. Teukolsky, W. Vetterling, and B. Flannery, *Numerical Recipes* (Cambridge University, 2007).
20. D. Kelly, B. Hennely, N. Pandey, T. Naughton, and W. Rhodes, "Resolution limits in practical digital holographic systems," Opt. Eng. **48**, 095801 (2009).
21. N. Verrier and M. Atlan, "Off-axis digital hologram reconstruction: some practical considerations," Appl. Opt. **50**, H136–H146 (2011).
22. P. Picart and P. Tankam, "Analysis and adaptation of convolution algorithms to reconstruct extended objects in digital holography," Appl. Opt. **52**, A240–A253 (2013).
23. L. Williams, G. Nehmetallah, R. Aylo, and P. P. Banerjee, "Near-field Fresnel reconstruction of digital holograms," in *OSA Digital Holography Topical Meeting* (Optical Society of America, 2014).
24. P. P. Banerjee and T.-C. Poon, *Principles of Applied Optics* (CRC Press, 2001). Fresnel transform Eq. (3.24).
25. P. Banerjee, H. Liu, and L. Williams, "Experimental evaluation of digital holographic reconstruction using compressive sensing," Proc. SPIE **9006**, 90060Y (2014).
26. P. Ferraro, S. De Nicola, G. Coppola, A. Finizio, D. Alfieri, and G. Pierattini, "Controlling image size as a function of distance and wavelength in Fresnel-transform reconstruction of digital holograms," Opt. Lett. **29**, 854–856 (2004).
27. M. Hillenbrand, D. P. Kelly, and S. Sinzinger, "Numerical solution of nonparaxial scalar diffraction integrals for focused fields," J. Opt. Soc. Am. A **31**, 1832–1841 (2014).
28. J. P. Liu, "Controlling the aliasing by zero-padding in the digital calculation of the scalar diffraction," J. Opt. Soc. Am. A **29**, 1956–1964 (2012).
29. L. Williams, P. Banerjee, G. Nehmetallah, and S. Praharaj, "Holographic volume displacement calculations via multiwavelength digital holography," Appl. Opt. **53**, 1597–1603 (2014).
30. L. Williams, G. Nehmetallah, and P. Banerjee, "Digital tomographic compressive holographic reconstruction of three-dimensional objects in transmissive and reflective geometries," Appl. Opt. **52**, 1702–1710 (2013).